Electronic Supplementary Information

Inkjet-Printed Micro-Calibration Standards for Ultraquantitative Raman Spectral Cytometry

Vernon LaLone, Maria V. Fawaz, Jomar Morales-Mercado, Márcio A. Mourão, Catherine S. Snyder, Sang Y. Kim, Anish Tuteja, Geeta Mehta, Andrew P. Lieberman, Theodore J. Standiford, Krishnan Raghavendran, Kerby Shedden, Anna Schwendeman, Kathleen A. Stringer, and Gus R. Rosania*

Corresponding Author

* E-mail: grosania@umich.edu

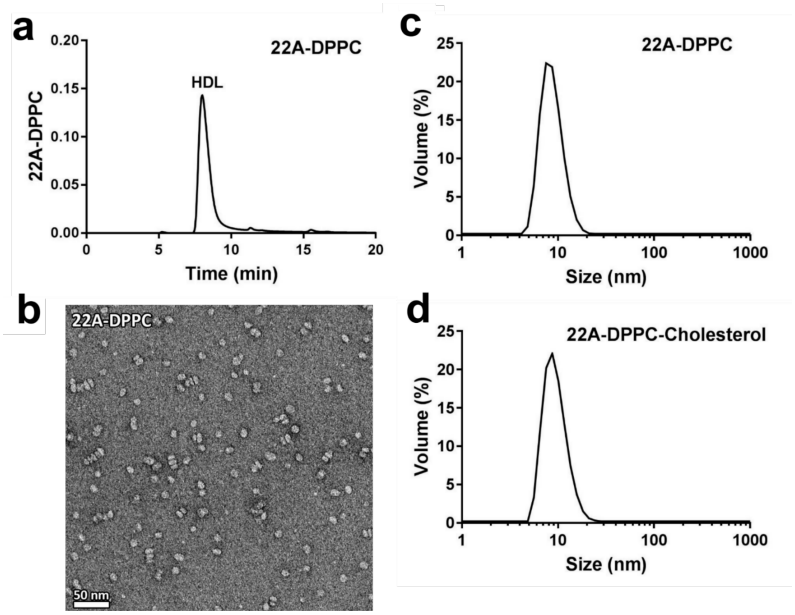

Figure S1. Characterization of 22A-DPPC and 22A-DPPC-Cholesterol HDLs**.** (a) The purity of synthetic HDL formulations was assessed using gel permeation chromatography, (b) morphology was analyzed by transition electron microscopy, and (c,d) particle size distribution was determined by dynamic light scattering; particle sizes were calculated as volume intensity averages (n=3).

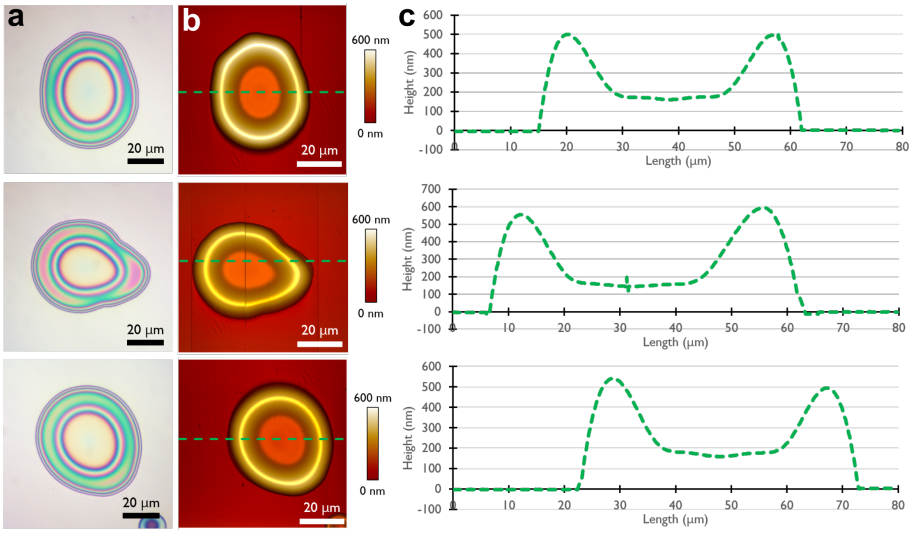

Figure S2. (a) Reflected brightfield images of 1000pg albumin micro-calibration standards on silicon chips and (b) corresponding AFM topographical profiles with cross-section marked in green dashed line (c).

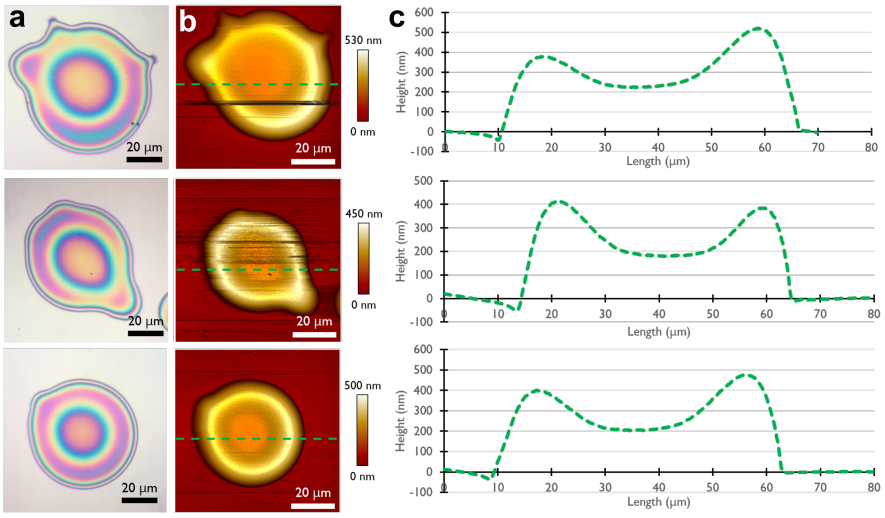

Figure S3. (a) Reflected brightfield images of 900pg HDL micro-calibration standards (each containing 600pg of lipid and 300pg of peptide 22A) on silicon chips and (b) corresponding AFM topographical profiles with cross-section marked in green dashed line (c).

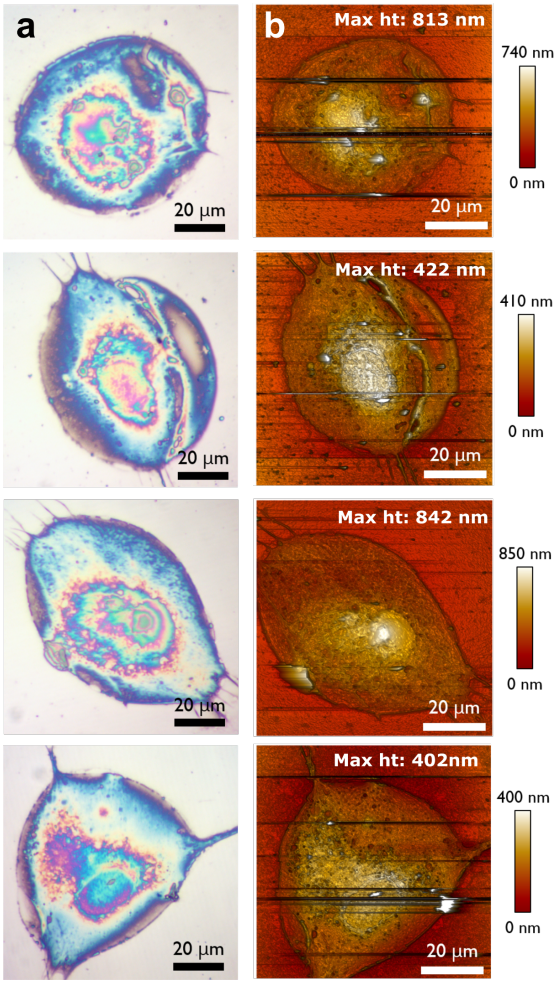

Figure S4. (a) Reflected brightfield images of fibroblast cell preparations on silicon chips and (b) corresponding AFM topographical profiles.

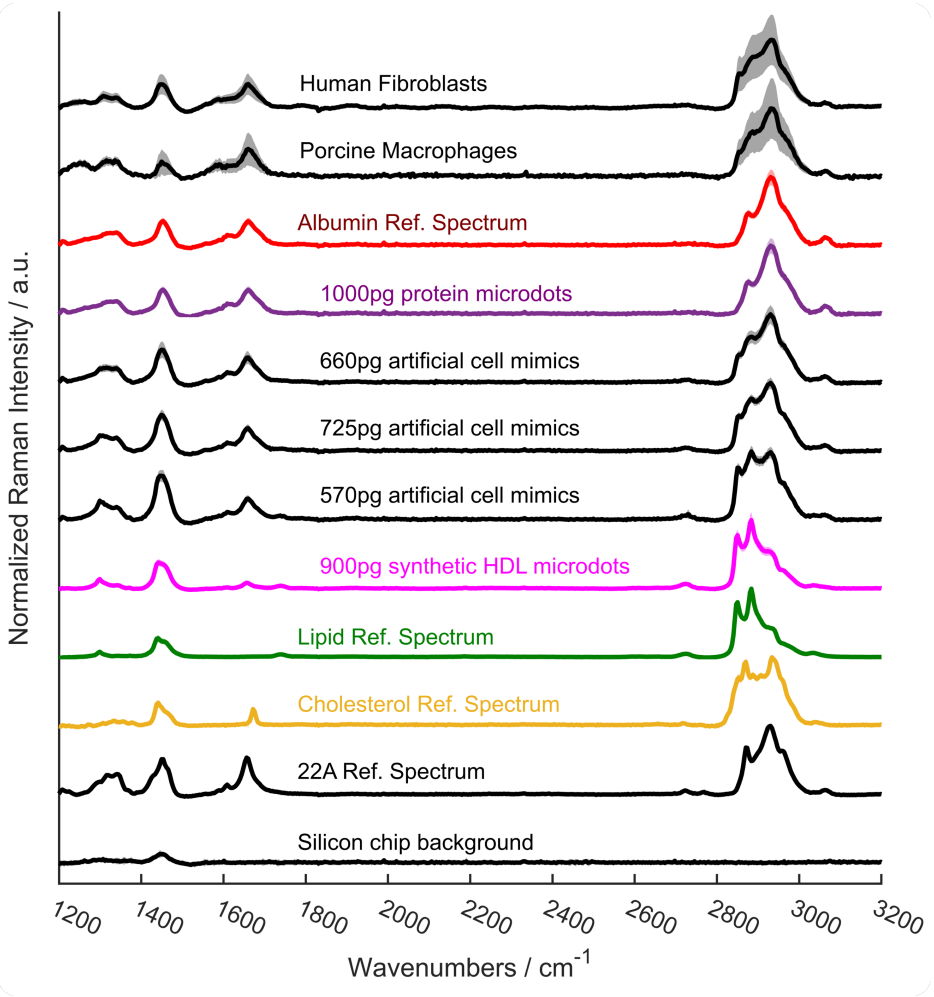

Figure S5. Raman spectral overlay of all major signal contributors including cell samples, pure component reference materials, and calibration micro-calibration standards; spectra shown are averages with standard deviation shown in shadow.

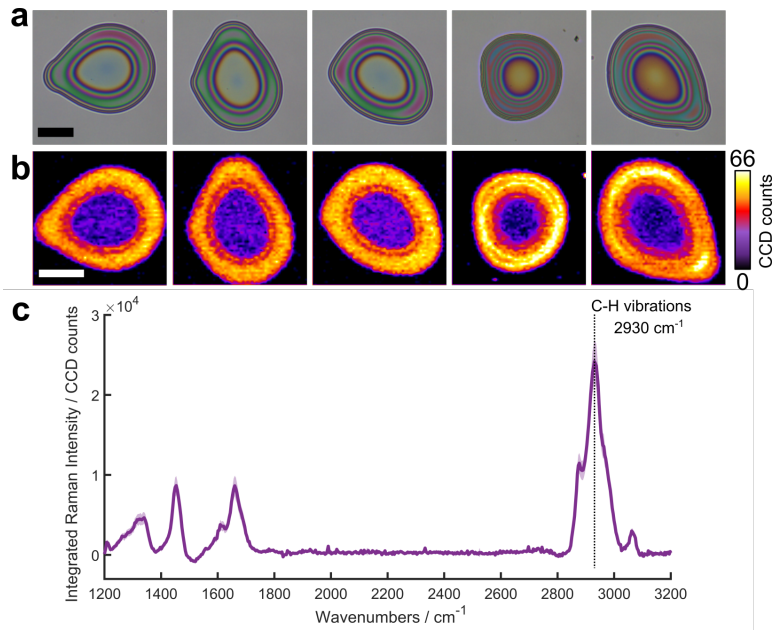

Figure S6. (a) Reflected brightfield images of 1000pg albumin micro-calibration standards on silicon chips and (b) corresponding Raman area scans for each showing signal intensity at 2930cm^{-1} and revealing material distribution; scale bars: 20µm. (c) Average integrated Raman spectrum (standard deviation shown by shadow) for the 1000pg micro-calibration standard dataset.

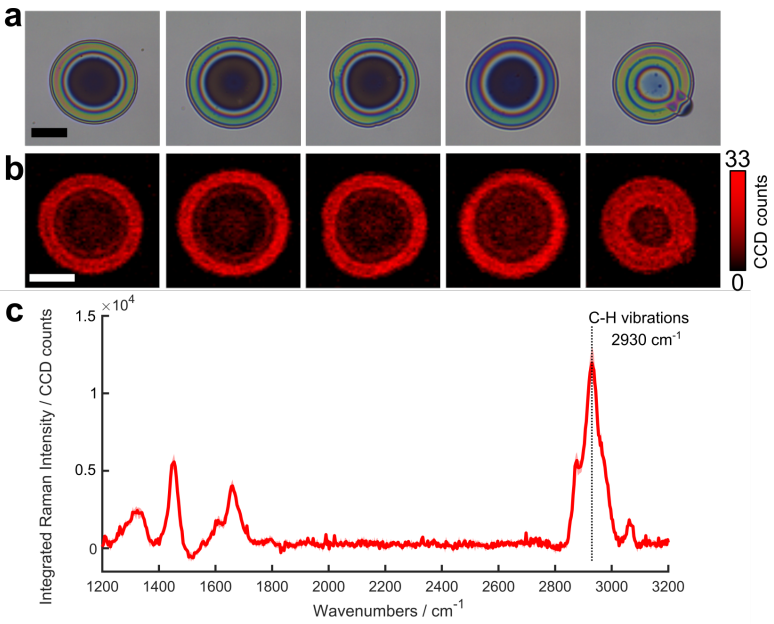

Figure S7. (a) Reflected brightfield images of 500pg albumin micro-calibration standards on silicon chips and (b) corresponding Raman area scans showing signal intensity at 2930cm^{-1} and revealing material distribution; scale bars: 20µm. (c) Average integrated Raman spectrum (standard deviation shown by shadow) for the 500pg micro-calibration standard dataset.

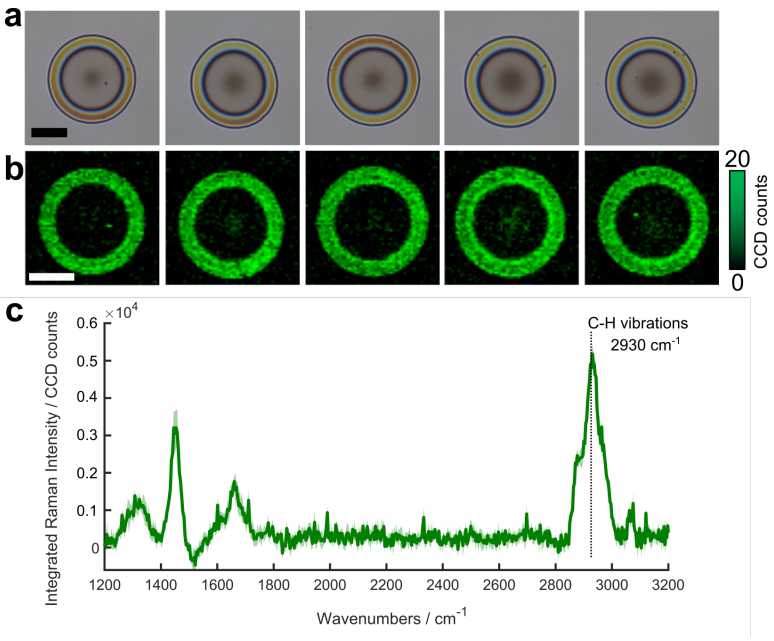

Figure S8. (a) Reflected brightfield images of 250pg albumin micro-calibration standards on silicon chips and (b) corresponding Raman area scans for each showing signal intensity at 2930cm^{-1} and revealing material distribution; scale bars: 20µm. (c) Average integrated Raman spectrum (standard deviation shown by shadow) for the 250pg micro-calibration standard dataset.

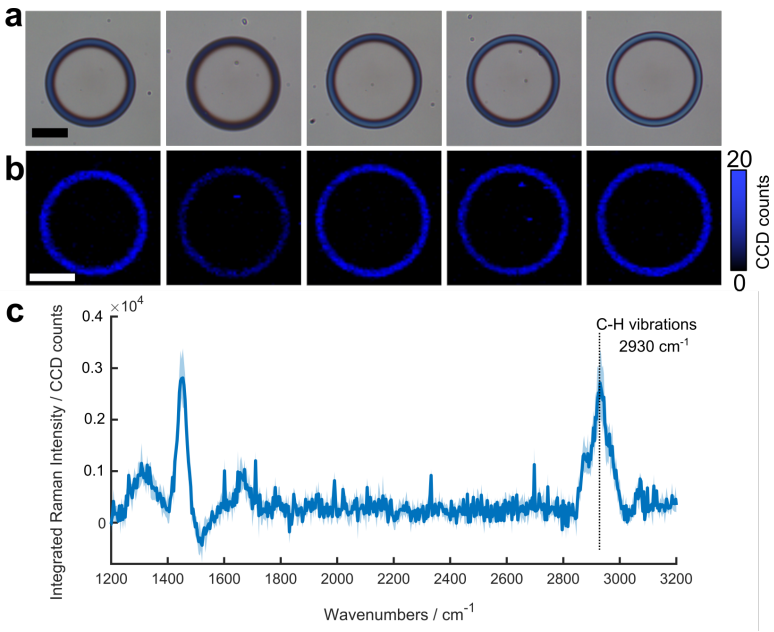

Figure S9. (a) Reflected brightfield images of 100pg albumin micro-calibration standards on silicon chips and (b) corresponding Raman area scans for each showing signal intensity at 2930cm^{-1} and revealing material distribution; scale bars: 20µm. (c) Average integrated Raman spectrum (standard deviation shown by shadow) for the 100pg micro-calibration standard dataset.

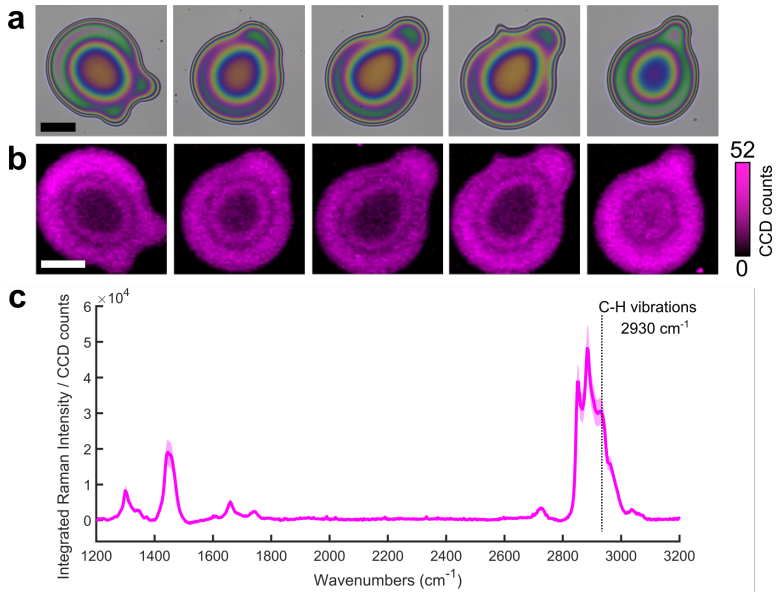

Figure S10. (a) Reflected brightfield images of 900pg HDL micro-calibration standards (each containing 600pg of lipid) on silicon chips and (b) corresponding Raman area scans for each showing signal intensity at 2930cm^{-1} and revealing material distribution; scale bars: 20μm. (c) Average integrated Raman spectrum (standard deviation shown by shadow) for the 900pg micro-calibration standard dataset.

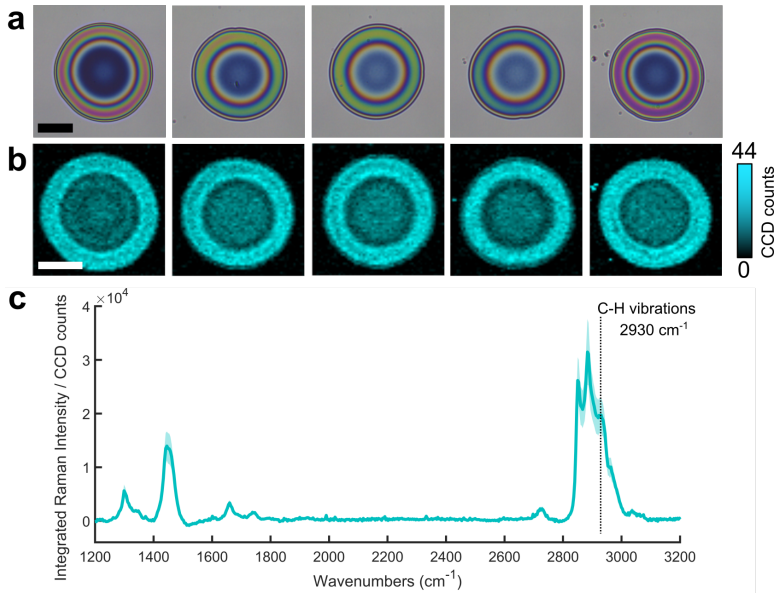

Figure S11. (a) Reflected brightfield images of 450pg HDL micro-calibration standards (each containing 300pg of lipid) on silicon chips and (b) corresponding Raman area scans for each showing signal intensity at 2930cm^{-1} and revealing material distribution; scale bars: 20µm. (c) Average integrated Raman spectrum (standard deviation shown by shadow) for the 450pg micro-calibration standard dataset.

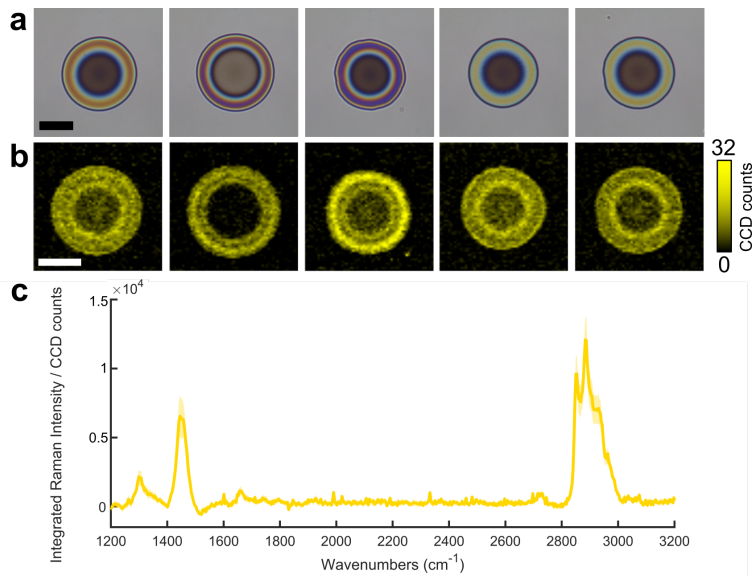

Figure S12. (a) Reflected brightfield images of 225pg HDL micro-calibration standards (each containing 150pg of lipid) on silicon chips and (b) corresponding Raman area scans for each showing signal intensity at 2930cm^{-1} and revealing material distribution; scale bars: 20μm. (c) Average integrated Raman spectrum (standard deviation shown by shadow) for the 225pg micro-calibration standard dataset.

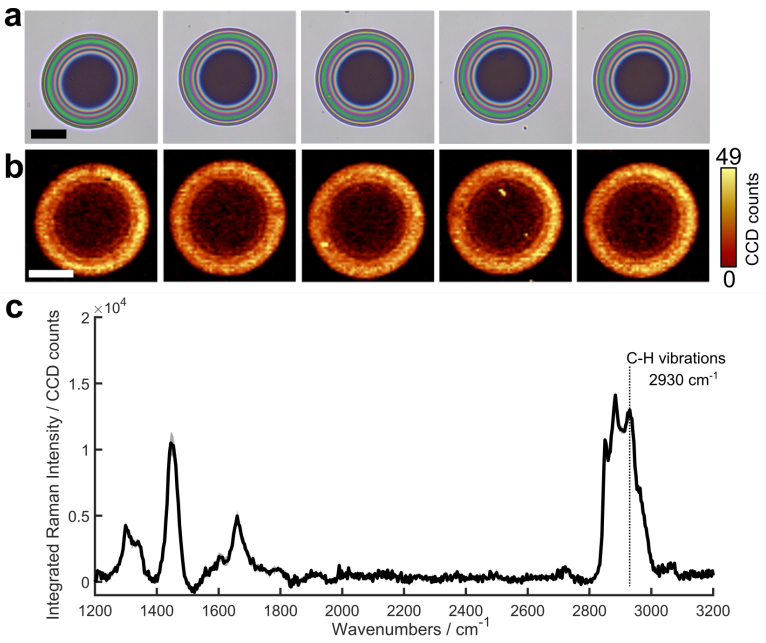

Figure S13. (a) Reflected brightfield images of 570pg mixed composition micro-calibration standards (each containing 250pg of albumin, 200pg of lipid, 100pg of peptide 22A, and 20pg of cholesterol) on silicon chips and (b) corresponding Raman area scans for each showing signal intensity at 2930cm^{-1} and revealing material distribution; scale bars: 20μm. (c) Average integrated Raman spectrum (standard deviation shown by shadow) for the 570pg micro-calibration standard dataset.

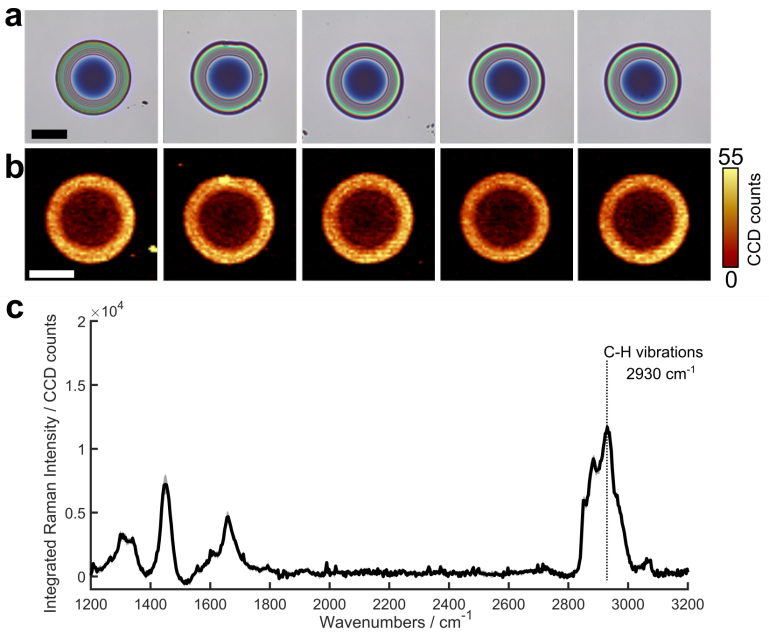

Figure S14. (a) Reflected brightfield images of 725pg mixed composition micro-calibration standards (each containing 500pg of albumin, 150pg of lipid, and 75pg of peptide 22A) on silicon chips and (b) corresponding Raman area scans for each showing signal intensity at 2930cm^{-1} and revealing material distribution; scale bars: 20μm. (c) Average integrated Raman spectrum (standard deviation shown by shadow) for the 725pg micro-calibration standard dataset.

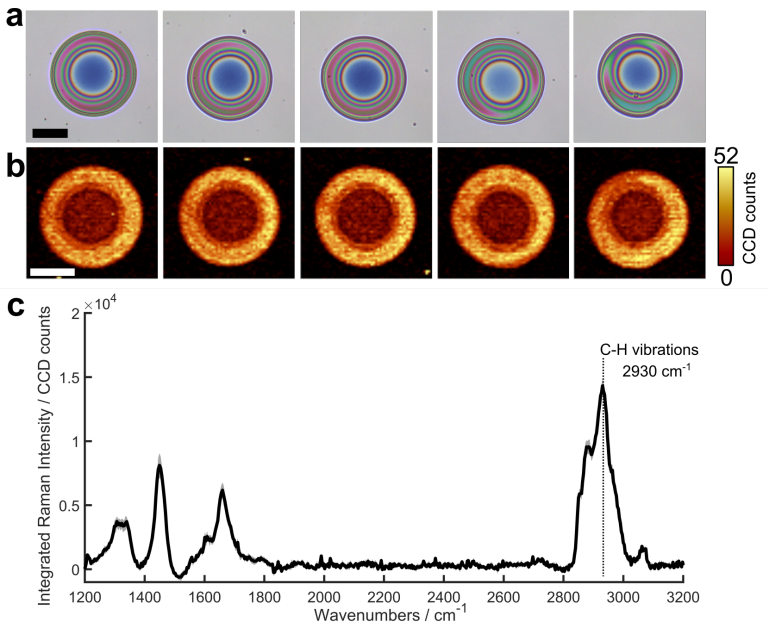

Figure S15. (a) Reflected brightfield images of 660pg mixed composition micro-calibration standards (each containing 500pg of albumin, 100pg of lipid, 50pg of peptide 22A, and 10pg of cholesterol) on silicon chips and (b) corresponding Raman area scans for each showing signal intensity at 2930cm^{-1} and revealing material distribution; scale bars: 20μm. (c) Average integrated Raman spectrum (standard deviation shown by shadow) for the 660pg micro-calibration standard dataset.

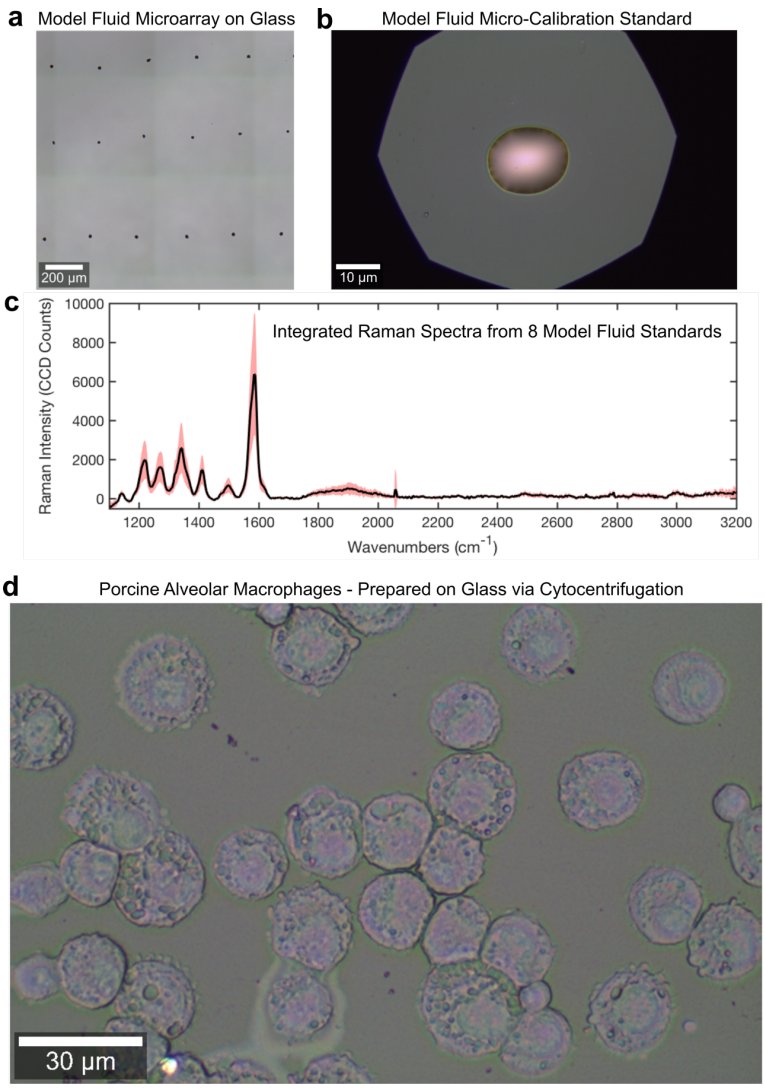

Figure S16. Preliminary feasibility testing for inkjet printing and cell preparation on glass slides. (a) Reflected brightfield image of inkjet-printed model fluid microarray on glass slide, (b) reflected brightfield image of a single model fluid micro-calibration sample, and (c) integrated Raman spectra acquire from 8 different model fluid samples. (d) Reflected brightfield image of untreated porcine alveolar macrophages prepared on glass slides via cytocentrifugation.

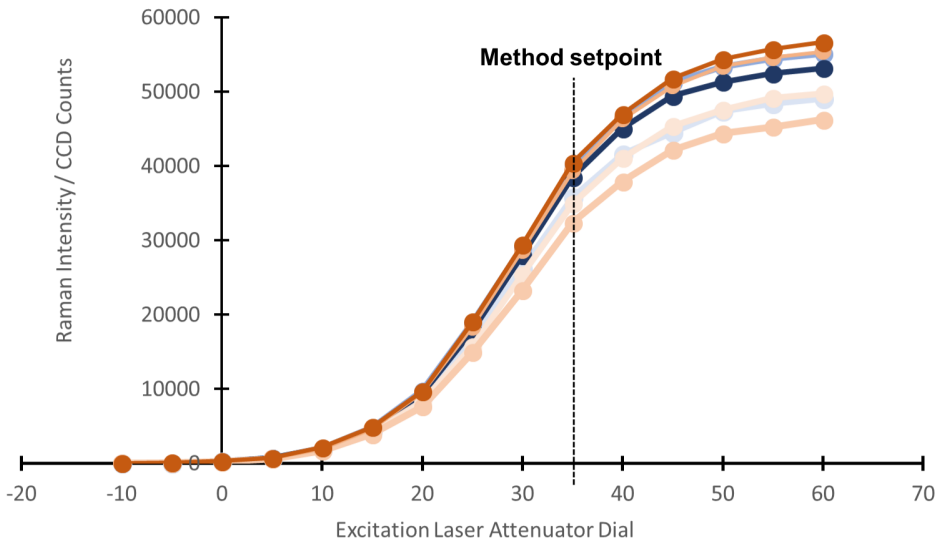

Figure S17. Instrument daily check performance curves (different colors/shades respectively represent different days/times); the laser is focused onto a clean surface of silicon chip and the z-plane is adjusted to acquire the optimal, or greatest, Raman signal intensity at 521cm^{-1} (the major Raman peak of silicon). The excitation laser attenuator dial is adjusted from completely closed to completely open in increments shown on dial and single spectra are acquired at each interval. By reporting the Raman intensity at 521cm^{-1} (shown on y-axis), the instrument performance was assessed daily. Instrument performance drift can be quantitatively measured at the method setpoint (the excitation intensity used for all Raman measurements reported in this project).

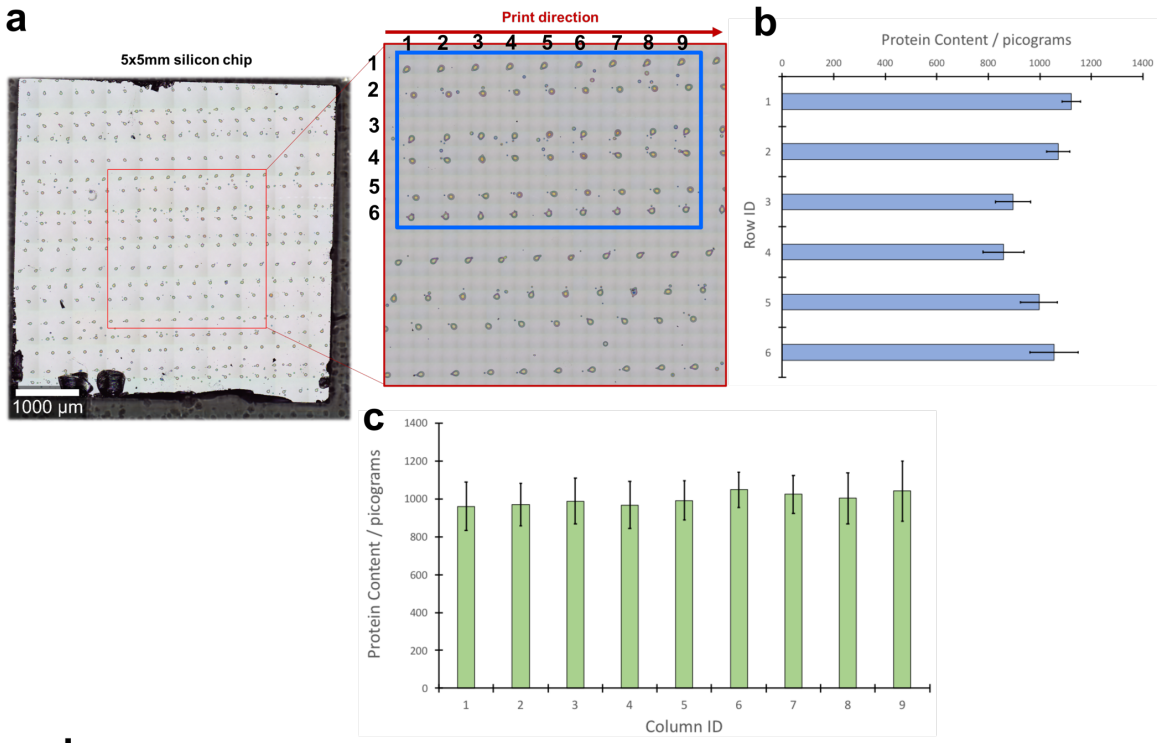

d

	1	2	3	4	5	6	7	8	9	Average	SD
1	1098	1100	1164	1082	1097	1119	1132	1120	1190	1122	35
2	1111	1021	1041	1079	1046	1139	1075	1009	1122	1071	46
3	871	893	912	839	1023	875	988	837	824	896	69
4	816	785	810	870	817	1055	847	850	880	859	80
5	1004	1006	972	854	921	1049	1073	1052	1045	997	72
6	867	1015	1035	1081	1051	1062	1032	1158	1195	1055	93
Average	961	970	989	967	993	1050	1025	1004	1043		
SD	127	112	121	124	104	93	99	135	158		

Figure S18. (a) Error analysis approach for 1000pg albumin microarray; 54 separate micro-calibration standards were analyzed via Raman microanalysis and the protein content (reported in units of picograms) was reported for each (b) row, (c) column, and (d) summarized in data table for each individual micro-calibration standard.

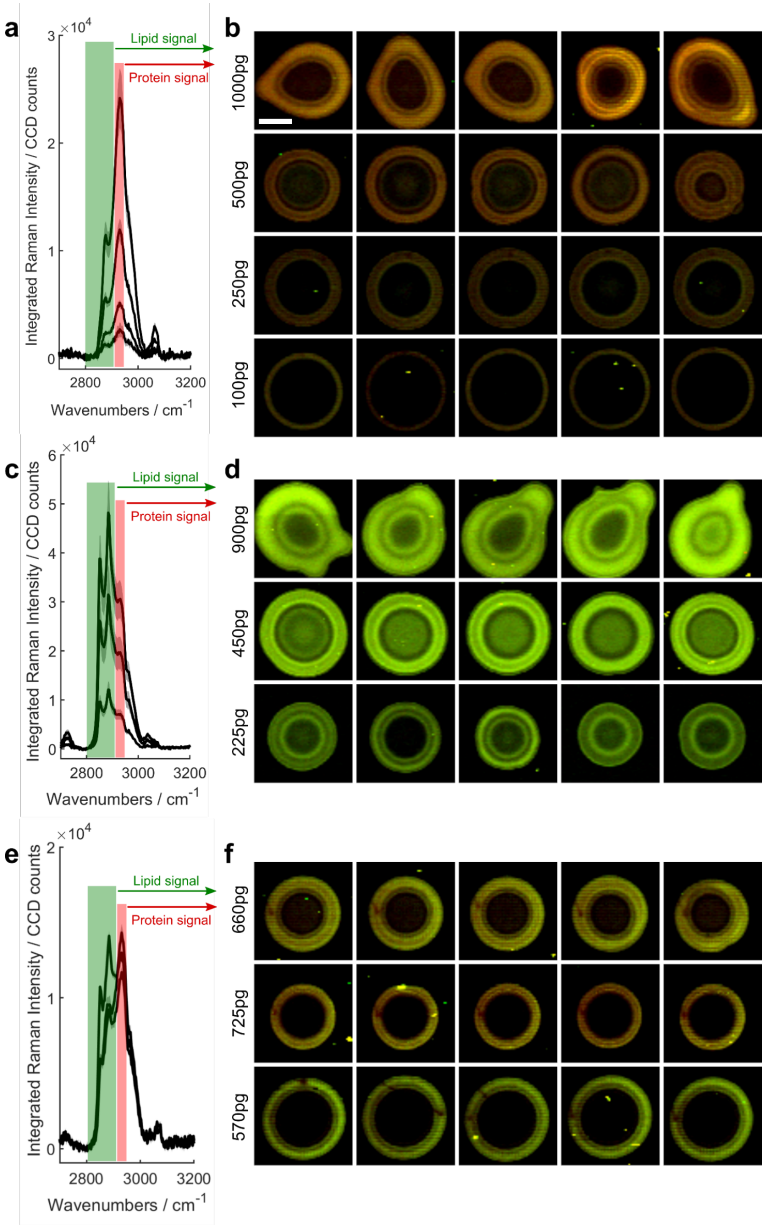

Figure S19. Multi-band Raman images of (a,b) protein, (c,d) HDL, and (e,f) mimic cell micro-calibration standards generated from Raman calibration datasets used for fibroblast quantitation. Scale bar: 20μm.

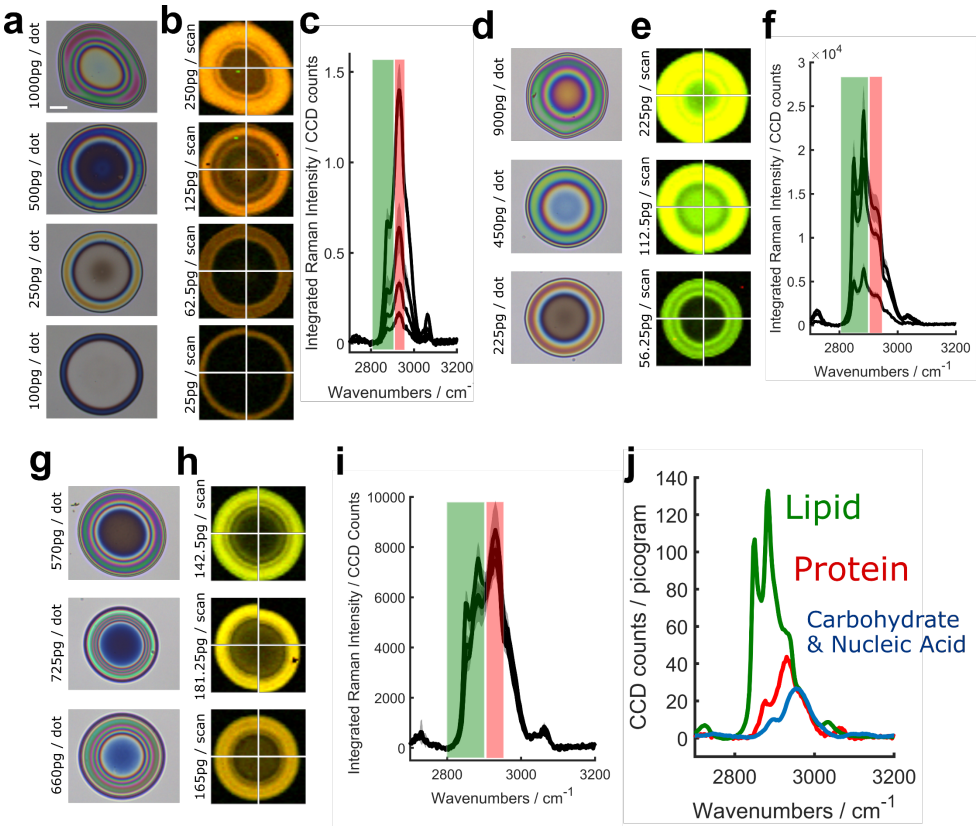

Figure S20. Quartered calibration micro-calibration standard measurements for quantitative calibration of alveolar macrophage datasets; (a-c) protein micro-calibration standard brightfield images (scale bar:20μm), multi-band Raman images generated from 25x25μm area scans, and integrated Raman spectra. (d-f) HDL micro-calibration standard brightfield images (scale bar:20μm), multi-band Raman images generated from 25x25μm area scans, and integrated Raman spectra. (g-i) mixed composition micro-calibration standard brightfield images (scale bar:20μm), multi-band Raman images generated from 25x25μm area scans, and integrated Raman spectra. (j) Ultraquantitative pure component reference spectra used for linear combination modelling of alveolar macrophage dataset.

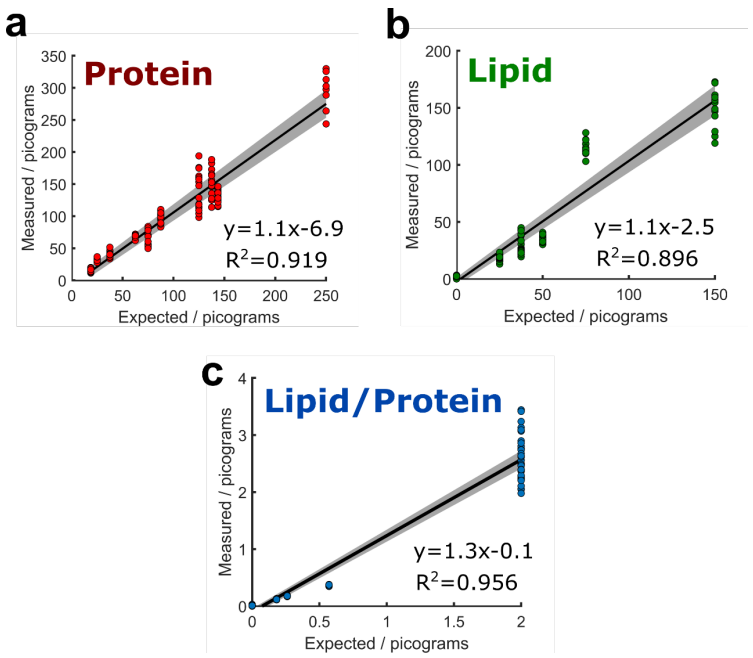

Figure S21. Quartered calibration micro-calibration standard measurements for quantitative calibration of alveolar macrophage datasets; linear regression of measured component content in relation to expected amount for protein (a), lipid (b), and lipid-to-protein ratio (c) including measured values from entire calibration dataset; shaded regions represent 95% confidence interval for measurement accuracy.

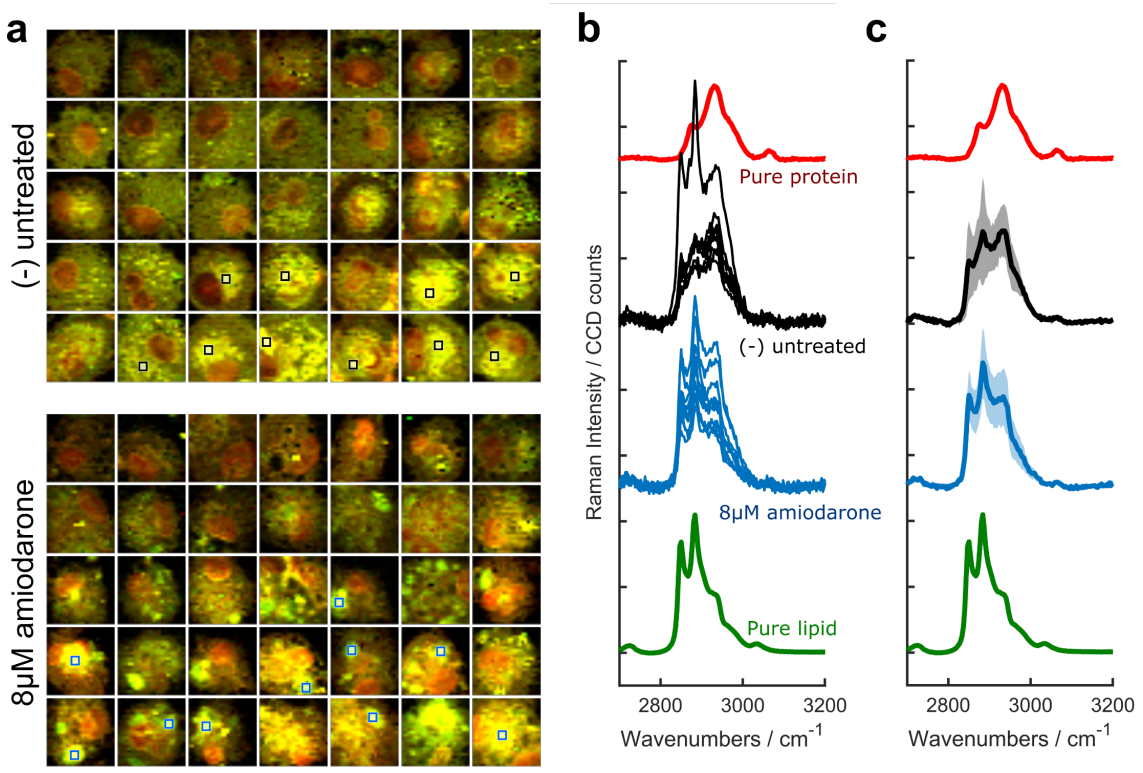

Figure S22. (a) Multi-band Raman images of alveolar macrophage Raman datasets; each scan is 25x25μm. (b) 3x3μm average spectra extracted from lipid-rich inclusions of 10 most lipid-laden cells from each population; pure protein and lipid (DPPC) reference spectra overlay. (c) Average+/-SD (shown in shadow) of each group of extracted spectra.

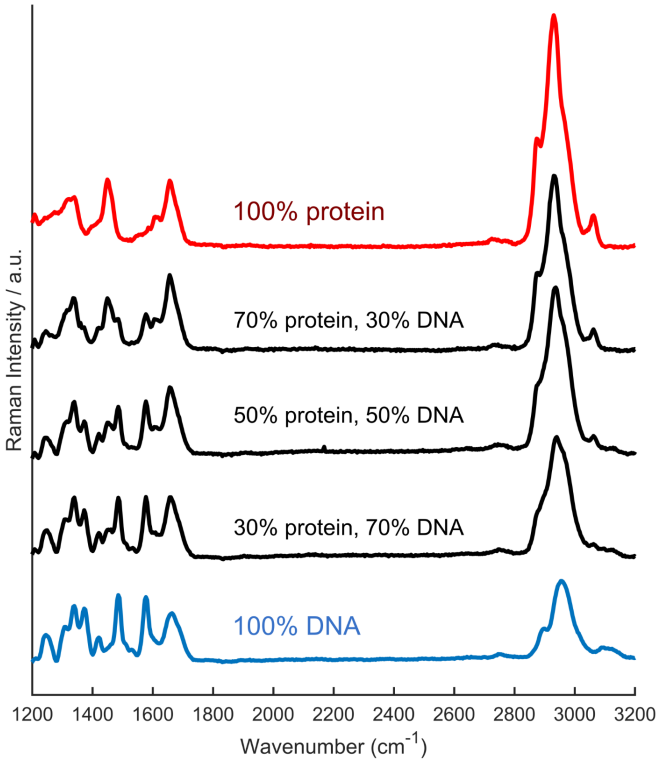

Figure S23. Stoichiometric mixtures of albumin and DNA used to experimentally determine "carbohydrate & nucleic acid" ultraquantitative reference spectra scaling.

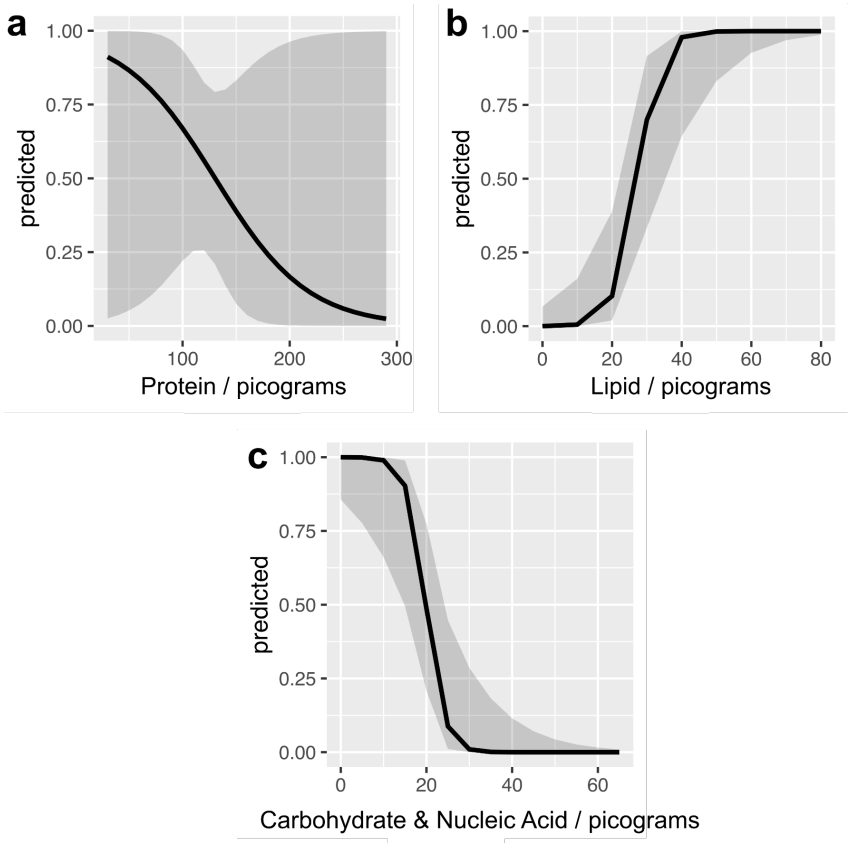

Figure S24. Logistic regression results for alveolar macrophage ultraquantitative dataset; predictive probability plots for (a) protein, (b) lipid, and (c) carbohydrate and nucleic acid.

Table S1. Logistic regression model results for alveolar macrophage ultraquantitative dataset (using picogram measurements as predictors).

	Estimate	Std. Error	z value	p-value
Intercept	3.73838145	1.59365893	2.3457852	0.018987049
Protein	-0.02320455	0.03158227	-0.7347335	0.462501832
Lipid	0.30189391	0.10791507	2.7975140	0.005149754
Carbohydrate & Nucleic Acid	-0.45733076	0.18154032	-2.5191691	0.011763215

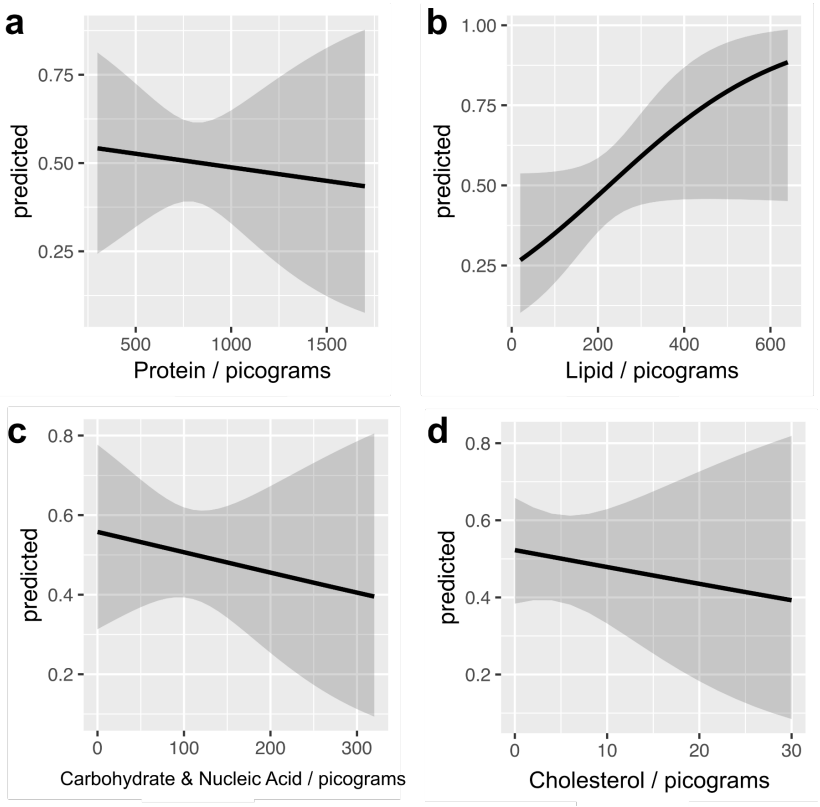

Figure S25. Logistic regression results for fibroblast ultraquantitative dataset; predictive probability plots for (a) protein, (b) lipid, (c) carbohydrate and nucleic acid, and (d) cholesterol measurements.

Table S2. Logistic regression model results for fibroblast ultraquantitative dataset (using picogram measurements as predictors).

	Estimate	Std. Error	z value	p-value
Intercept	-0.567338105	0.780569701	-0.7268257	0.46733275
Protein	-0.000308520	0.001242250	-0.2483558	0.80385910
Lipid	0.004917963	0.002678185	1.8363047	0.06631261
Cholesterol	-0.017560972	0.037796071	-0.4646243	0.64220055
Carbohydrate & Nucleic Acid	-0.002052581	0.004299290	-0.4774232	0.63306080

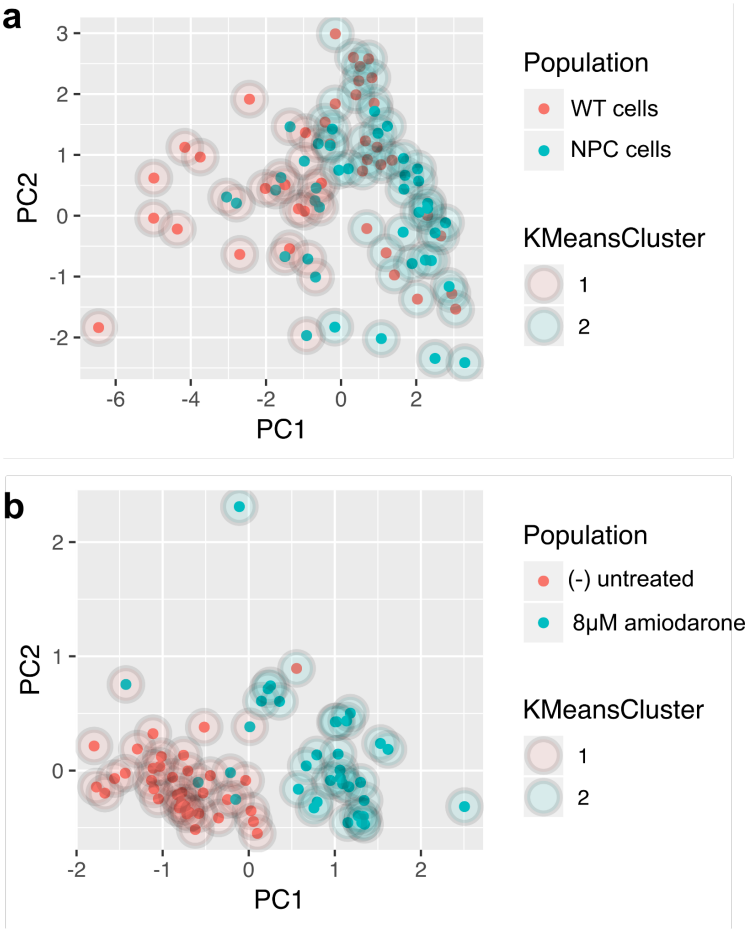

Figure S26. K-means clustering of PCA results datasets (PC scores) for (a) fibroblasts and (b) alveolar macrophages.